

INTERFACIAL CRACKS IN PLATES: A THREE-DIMENSIONAL NUMERICAL INVESTIGATION

YEONG JOO LEE† and A. J. ROSAKIS

Graduate Aeronautical Laboratories, California Institute of Technology, Pasadena, CA 91125,
U.S.A.

(Received 9 October 1992; in revised form 19 April 1993)

Abstract—The three-dimensional field at a crack front in a bimaterial interface is investigated in order to identify relevant fracture parameters in thin plate laboratory specimens. Existence of plane stress K -dominance is necessary for the proper analysis of experimental data, which can be obtained directly from the crack-tip field by optical methods. The analysis of the three-dimensional structure of the crack-tip field presented here is performed in relation to the three-point bend specimen geometry used in the experiments described in Lee and Rosakis (1993), *Interfacial cracks in plates: an experimental investigation* (in preparation). It is well known that the three-dimensional field at the vicinity of a crack in a plate composed of a homogeneous material extends over a half-plate thickness from the crack front. However in a bimaterial fracture specimen, in addition to the singular field at the crack tip, mismatch of material properties along the interface induces a strip of three-dimensionality extending along the bimaterial interface ahead of the crack tip. The extent of the three-dimensional zone and a critical discussion of the zone of K -dominance are presented. The relation between the stress intensity factors in the remote plane stress K -field and the stress intensity factors inside the near-tip plane strain K -field is also derived by means of a separate boundary-layer type of numerical analysis. Finally, a means of scaling the results obtained by experimentation in thin plate specimens of a specific thickness-to-plate specimens of any thickness is proposed.

1. INTRODUCTION

The scientific estimation of the toughness of interfacial cracks in bimaterial combinations is essential in the analysis of failure mechanisms in advanced materials such as fiber-reinforced composites and ceramic composites. Little is known about the three-dimensional structure of interfacial cracks in thin bimaterial plates, while the issue of the existence and region of dominance of a plane stress K -field has never been explored. In this investigation these issues are studied in relation to the three-point bend specimen geometry. This choice is partially motivated by the projected use of such a geometry in dynamic fracture experiments [see Rosakis *et al.* (1991)].

Detailed three-dimensional computations are necessary for supporting not only ongoing quasi-static fracture experiments but also dynamic ones. A major purpose of such calculations is to establish the regions near the crack tip where experimental measurements can be performed and analysed with maximum accuracy. Parsons *et al.* (1986) and Krishnaswami *et al.* (1991) investigated the three-dimensional structure of static and dynamically loaded cracks in homogeneous elastic materials. Nakamura and Parks (1988, 1989) studied the three-dimensional aspects of cracks in homogeneous elastic plates under mode I and II loading conditions, respectively. They observed that the mode III component of the stress intensity factor increases monotonically from the mid-plane of the plate and appears to be infinite at the free surface under remote pure mode II loading conditions. Narasimhan and Rosakis (1988) observed three-dimensional effects near a crack tip in a thin ductile plate. They concluded that many of the discrepancies in the experimental literature might arise from the lack of the establishment of an underlying asymptotic field which is customarily assumed in the interpretation of the experimental data.

However, very limited research has been devoted to the investigation of the role of three-dimensionality in interfacial cracks. In this case three-dimensional effects in the vicinity of an interfacial crack are not only caused by the presence of the crack itself but they are enhanced by the presence of the material mismatch along the interface. Recently,

† Present address: Dow Chemical Company, 1776 Building, Midland, MI 48674, U.S.A.

Gharhmani and Shih (1990) and Barsoum and Chen (1991) analysed the corner singularity of bimetals by using the finite element method. They showed that many material combinations do not exhibit oscillatory fields near the corner singularity and that in such cases, the singularities of both the symmetric and anti-symmetric modes range from 0.5 to 0.75 as the material mismatch becomes larger. Even though the corner can serve as a nucleation site in an initially straight crack front and the corner-singular field may crucially influence the resulting shape of the crack front after initiation, it is energetically unlikely that it will play an important role in the whole fracture process through the thickness. This is true since the zone size is too small and the well-developed plateau of K -values through the thickness dominates. In addition to the singularity at the crack front and the corner singularities at the intersection of the crack front with the free surface, other singular fields also appear along the line of intersection of the interface plane and the free surface ahead of the crack tip in bimetals due to material mismatch. Bogy (1971) obtained the strength of this singularity by solving a series of eigenvalue problems. The singularity of this interfacial wedge field (wedge angle is zero) is weaker than the crack front singularity for any bimaterial combination and it is not oscillatory. Recently, Nakamura (1991) presented a three-dimensional analysis of a center-cracked panel bimaterial fracture specimen. In his analysis, the shear moduli and Poisson ratios of the two different materials were particularly chosen to suppress the usually oscillatory stress field near the crack tip which is governed by mostly plane strain conditions. In his investigation, emphasis was given to the near-tip *plane strain* region. In our work the motivation is entirely different. We are interested in providing numerical support to specific sets of experiments. In particular, the first goal of this work is related to the investigation of the accuracy of experimental data analysis and fracture parameter extraction in three-point bend bimaterial plates of different dimensions. This is achieved by numerically analysing the extent of the near-tip field three-dimensional zone and by estimating the size of plane stress K -dominance in plates of a variety of crack lengths and thicknesses. This seems to be a necessary step prior to experimentation. The second goal is to establish a relationship between the far-field, plane stress, complex stress intensity factor and the near-tip, plane strain, equivalent. In thin plates, two asymptotic fields emanate from the crack tip. One is the plane strain K -field which is located very near the crack tip (within the three-dimensional zone). Another is the plane stress K -field which surrounds the near-tip three-dimensional zone. The plane strain zone near the tip is too small to be captured experimentally. Thus, a conversion process of the experimentally observed, plane stress, stress intensity factor, to the near-tip, plane strain, stress intensity factor, is necessary to characterize the interfacial toughness of bimetals. Because of the three-dimensional nature of the fields, all three components of stress intensity factor depending on the mixity of the external loading, are presented as an outcome of three-dimensional effects. The deviation from the K -field due to the corner singularity at a point sufficiently close to the normal intersection of a crack front and a free surface, is also observed.

Coherent Gradient Sensing (CGS) fringe patterns, which were experimentally obtained in Lee and Rosakis (1993), are compared with synthetically generated fringes from the three-dimensional finite element analysis. Preliminary CGS fringe data of dynamically propagating cracks in an elastic bimaterial (PMMA/aluminum) were recently reported by Tippur and Rosakis (1991) and Rosakis *et al.* (1991). Very high velocities of propagation along the interface were observed (80% of the Rayleigh wave speed of the less stiff material, PMMA). Since contrary to static experiments, it is very difficult to obtain fracture parameters of dynamically propagating cracks by boundary measurements, direct real-time measurements of stress or displacement fields near the crack tip by using optical techniques are necessary. Such techniques may include the optical method of caustics (Beinert *et al.*, 1981; Rosakis, 1992), the Stress Intensity Factor Tracer (Kim, 1985), Moiré interferometry (Post, 1987) and the Coherent Gradient Sensing (CGS) (Tippur *et al.*, 1991; Rosakis, 1993). This necessity of local measurements partially motivates the current investigation. Indeed, the static analysis presented here is an important first step to being able to analyse the data taken from the stress field near propagating cracks in dynamic experiments of the type described in Rosakis *et al.* (1991).

2. STATEMENT OF PROBLEM

The finite element calculations are designed to describe the three-dimensional nature of the near-tip stress field, to provide the boundary of the three-dimensional zone and to establish the region of dominance of the plane stress K -field surrounding this zone. Four different solutions are of interest here. These are the three-dimensional full-field and the plane stress two-dimensional full-field solutions, for the three-point bend specimen, as well as the corresponding plane strain and plane stress asymptotic solutions. The plane strain and plane stress asymptotic solutions provide approximations to the three-dimensional full-field solution at different regions near the crack tip. Such approximations allow for the extraction of fracture parameters from optical data obtained directly from the crack tip. The region of dominance of the plane strain asymptotic solution is confined very deeply inside the three-dimensional zone, where measurements are difficult. As a result, it is necessary to perform optical measurements outside the near-tip three-dimensional zone where a plane stress K -field may exist. Consequently, choice of a specimen geometry that could allow for the establishment of such a field is desirable. After we can measure plane stress K values from the experiments, they must be converted to local plane strain K values which are more likely to represent material properties when the crack initiates and grows. For this reason, in the latter part of this paper we perform a boundary-layer type of the three-dimensional calculation for the interfacial cracks in the bimaterial plates, which provides the relation between the far-field, plane stress, K value and the thickness average of the near-tip, plane strain, K value.

The asymptotic structure of the two-dimensional stress field of the interfacial cracks for the given bimaterials is expressed by three components of stress intensity factor in the following :

$$\sigma_{ij} = \frac{1}{\sqrt{2\pi r}} [\operatorname{Re} \{Kr^{ie}\} \Sigma_{ij}^1(\theta, \varepsilon) + \operatorname{Im} \{Kr^{ie}\} \Sigma_{ij}^2(\theta, \varepsilon) + K_3 \Sigma_{ij}^3(\theta)], \quad (1)$$

where r and θ are the crack tip polar coordinates, $K = |K| e^{i\psi}$ is the complex stress intensity factor for the coupled in-plane modes, K_3 is the mode 3 stress intensity factor, ψ designates the phase angle and $\Sigma_{ij}^{1,2,3}$ are the angular variations of stress components for each mode. The oscillatory index ε is defined in the following :

$$\varepsilon = \frac{1}{2\pi} \ln \left[\frac{\kappa_1 \mu_2 + \mu_1}{\kappa_2 \mu_1 + \mu_2} \right], \quad (2)$$

where $\kappa_\alpha = 3 - 4\nu_\alpha$ for plane strain and $\kappa_\alpha = (3 - \nu_\alpha)/(1 + \nu_\alpha)$ for plane stress, μ_α is the shear modulus, ν_α is the Poisson ratio and the subscripts 1 and 2 refer to the materials above and below the crack plane. If the in-plane dimension of the cracked plate is much larger than the thickness, it is possible that there is a plane stress K -field outside of the three-dimensional zone, coexisting with a plane strain K -field near the crack tip. Therefore, from now on, we will use ε_s as the oscillatory index under plane strain conditions and ε_σ as the oscillatory index under plane stress conditions in order to avoid confusion.

For the purpose of comparison with experimental results, material data of commercially available poly-methyl methacrylate (PMMA) (material 1) and Al 6061-T6 (material 2) are used in this computation. The adhesive on the PMMA/aluminum interface is the methyl methacrylate monomer (MMA) which polymerizes when it is mixed with a catalyst. This results in a bond material with stiffness similar to that of PMMA. In addition, the thickness of interface is very small so that we regard this problem as the perfectly bonded interface problem of the two materials and we neglect the third material, i.e. the polymerized MMA. Material properties of PMMA and aluminum are shown in Table 1. The ratio of the Young's moduli of an aluminum to a PMMA is so large, 25:1, that very large oscillatory indices, ε_σ and ε_s , are obtained as 0.098 and 0.068, respectively.

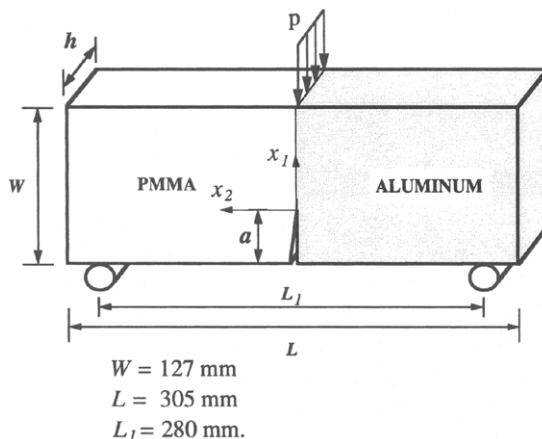


Fig. 1. Dimensions of PMMA/aluminum bimaterial three-point bend specimen and schematic description of loading.

3. PLANE STRESS K -FIELD

The initial set of finite element simulations of the three-point bend experiments are attempted under plane stress conditions in order to find the radial distance within which the asymptotic solution (K -field) can approximate the full-field solution within a certain tolerance. The loading system and the dimensions of specimens are schematically shown in Fig. 1. A unit load per unit plate thickness is imposed on the center of the top edge of the plate.

It is essential that the discretization near the crack tip must be such as to resolve the expected singular crack tip fields adequately. The mesh discretization shown in Fig. 2 consisting of 864 four-noded isoparametric quadrilateral elements (938 nodes) was found to be appropriate for the present investigation. As the crack length for the given specimen dimension varies, the configuration of the mesh changes by moving the location of the crack tip, while the number of elements is not changed. For the purpose of direct comparison

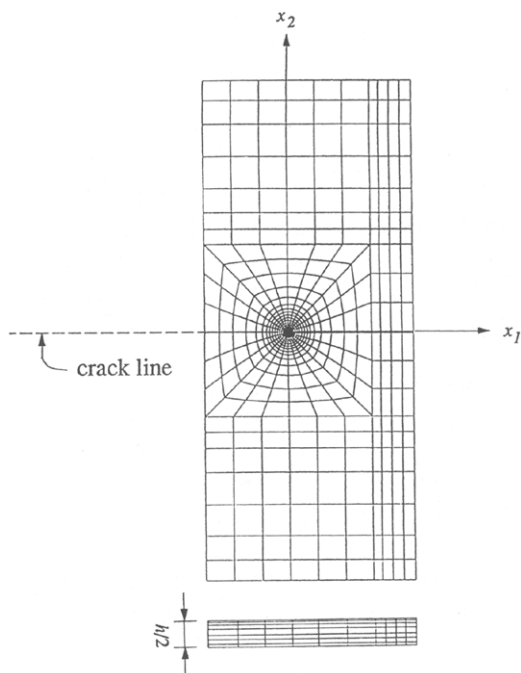


Fig. 2. The two-dimensional and three-dimensional finite element mesh.

SIF and Phase Angle with α/W

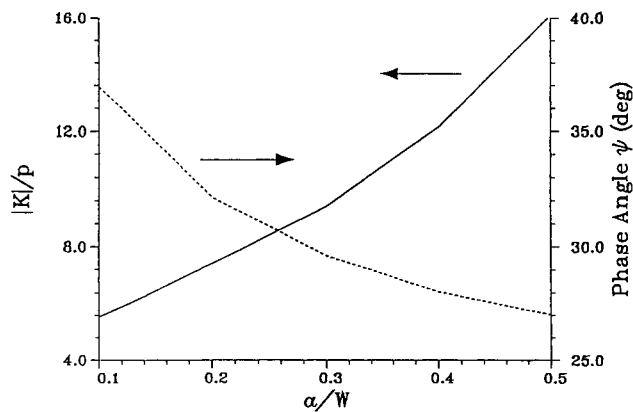


Fig. 3. The variation of the magnitude of the normalized stress intensity factor and phase angle with the crack length for given in-plane dimension under plane stress conditions.

with the experiments in our laboratory, we fix the in-plane dimensions of the specimen except the crack length. The specimen thickness also varies.

The in-plane stress intensity factors are calculated by the combination of the interaction energy formulation (Stern *et al.*, 1976; Yau *et al.*, 1980; Shih *et al.*, 1986) and the domain integral formulation (Nakamura *et al.*, 1986) as follows. Let the value of the interaction energy release rate be denoted as G_{int} , then

$$G_{int} = - \int_{A_0} \left[\sigma_{\alpha\beta} \epsilon_{\alpha\beta}^{aux} \frac{\partial q}{\partial x_1} - \sigma_{\alpha\beta} \frac{\partial u_{\alpha}^{aux}}{\partial x_1} \frac{\partial q}{\partial x_{\beta}} - \sigma_{\alpha\beta}^{aux} \frac{\partial u_{\alpha}}{\partial x_1} \frac{\partial q}{\partial x_{\beta}} \right] dA, \quad (3)$$

where Greek letters in subscripts range from 1 to 2, q is a continuous weighting function of position and the boundary of the domain (A_0) in the integration is arbitrary. The variables with the superscripts ‘‘aux’’ are the solutions of the auxiliary fields corresponding to the mode 1 and 2 plane stress asymptotic fields of the problem, satisfying the equilibrium equations and the traction-free conditions on the crack faces. This interaction energy release rate is a conservation energy integral and it is related to the stress intensity factors along the crack front line by :

$$G_{int} = \frac{2}{\bar{E} \cosh^2(\pi \epsilon_{\sigma})} [K_1 K_1^{aux} + K_2 K_2^{aux}], \quad (4)$$

where $K_{1,2}^{aux}$ are stress intensity factors for the auxiliary stress field. The effective Young’s modulus \bar{E} is defined in the following :

$$\frac{1}{\bar{E}} = \frac{1}{2} \left(\frac{1 - \nu_1^2}{E_1} + \frac{1 - \nu_2^2}{E_2} \right), \quad \frac{1}{2} \left(\frac{1 - \nu_1}{2\mu_1} + \frac{1 - \nu_2}{2\mu_2} \right), \quad (5)$$

where μ_s are shear moduli of each material. It is easy to extract each component of stress intensity factors by first numerically evaluating G_{int} , then inserting 1 in the corresponding component of stress intensity factors of the auxiliary stress field and neglecting the other component in eqn (4). The weighting function q is the cone-shaped function with value 1 at the crack tip and value 0 at the boundary of the domain.

In Fig. 3, the magnitude of the complex stress intensity factor per unit line force and the phase angle are shown according to the ratio of the crack length to the width of the plate. The magnitude of the stress intensity factor increases as the crack grows for the given

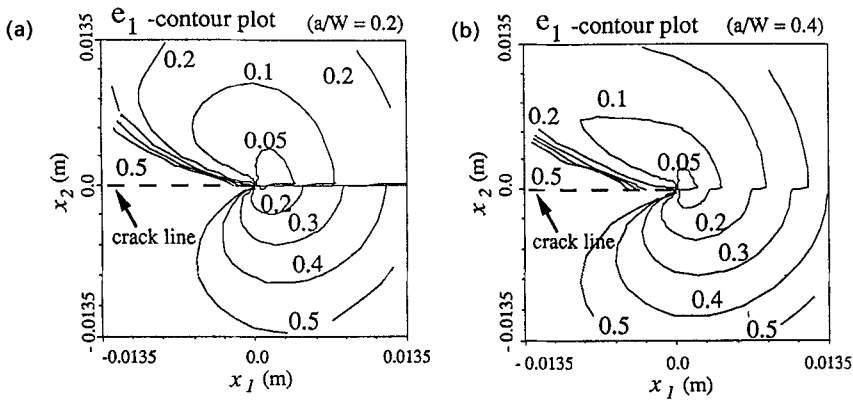


Fig. 4. The extent of the deviation (e_1) of the two-dimensional full field solution from the plane stress asymptotic solution. Contour levels of $e_1 = |\sigma - \sigma^A|/|\sigma^A|$ are illustrated: (a) $a/W = 0.2$, and (b) $a/W = 0.4$.

load, while the phase angle decreases. For the given range of the crack lengths, only a small change of phase angles, $27^\circ \sim 37^\circ$, is observed.

The extent of the difference between the two-dimensional plane stress full-field solution and the corresponding asymptotic K -field solution can be expressed by means of the following field quantity:

$$e_1 = \sqrt{\frac{(\sigma_{\alpha\beta} - \sigma_{\alpha\beta}^A)(\sigma_{\alpha\beta} - \sigma_{\alpha\beta}^A)}{\sigma_{\alpha\beta}^A \sigma_{\alpha\beta}^A}} \quad (\alpha = 1, 2), \quad (6)$$

where $\sigma_{\alpha\beta}$ and $\sigma_{\alpha\beta}^A$ are the stress components of the two-dimensional plane stress full-field solution and the asymptotic solution respectively and Einstein's summation convention is applied to the repeated subscripts. In Fig. 4, contour plots of this quantity for the cases of $a/W = 0.2$ and 0.4 are illustrated. It should be observed that the contour line of $e_1 = 0.1$ for $a/W = 0.2$ is further away from the crack tip than that for $a/W = 0.4$. We may expect that the stress state near the neutral axis of bending, which is supposed to be located near the center of the ligament, erodes the K -field as the crack length becomes longer for the given width of the ligament. Based on this information, the K -field expands until the crack length reaches 20% of the plate width and shrinks as the crack length becomes large.

In the experiments in optical techniques such as the Twyman-Green interferometry, the optical method of caustics and or the Coherent Gradient Sensing (CGS), each fringe in a plane stress region is proportional to the hydrostatic stresses or its gradient [see Rosakis (1992)]. As a result, we may take the value of the hydrostatic stress as a measure of the deviation of the full-field solution from the asymptotic solution. In order to quantify this deviation, we define the following field quantity involving only hydrostatic stress components as follows:

$$e_2 = \frac{\sigma_{\alpha\alpha} - \sigma_{\alpha\alpha}^A}{|\sigma_{\alpha\alpha}^A|} \quad (\alpha = 1, 2). \quad (7)$$

In Fig. 5, contours of e_2 for $a/W = 0.2$ and 0.4 are drawn respectively. The asymptotic solution agrees well with the full-field solution in the narrow band, which is centered at 135° from the crack line. For homogeneous materials, Tippur *et al.* (1991) also observed that the best fit of experimentally obtained CGS fringes to the synthetic CGS fringes of the asymptotic stress field was obtained along $120^\circ \sim 130^\circ$ in various values of a/W .

The above plane stress calculation establishes the outer boundary of the zone of K -dominance as viewed by means of the two deviation measures e_1 and e_2 . The inner boundary can only be obtained by comparison of the K -field to the fully three-dimensional calculation described in the next section.

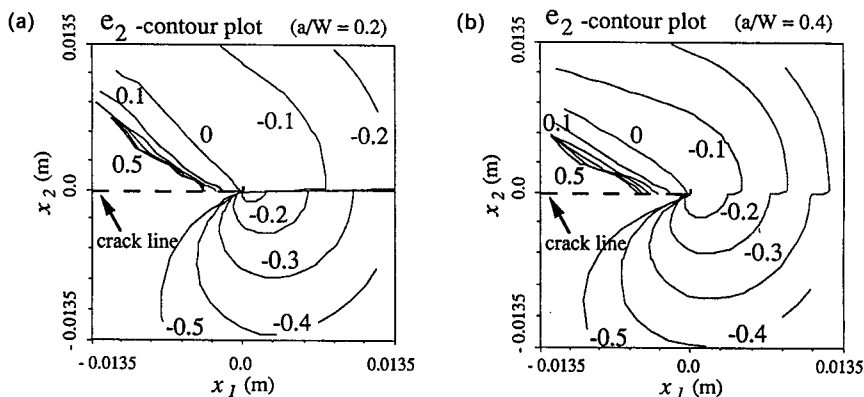


Fig. 5. The extent of the deviation (e_2) of the two-dimensional full-field solution from the plane stress asymptotic solution. Contour levels of $e_2 = (\sigma_{xx} - \sigma_{xx}^A) / |\sigma_{xx}^A|$ are illustrated: (a) $a/W = 0.2$, and (b) $a/W = 0.4$.

4. THREE-DIMENSIONAL STRESS FIELD

In this section, the extent of the three-dimensional zone near the interfacial plane as well as near the vicinity of the crack tip will be investigated for the three-point bend interfacial experiments.

In Fig. 2, one of the typical mesh geometries used in the three-dimensional analysis is shown. By using the symmetry to the midplane, we modeled only one half of the three-dimensional body. Seven layers of eight-noded hexagonal brick elements through half the thickness leading to 7 elements (8 nodes) were used. The in-plane layout is exactly the same as that used in the two-dimensional plane stress computation. Recognizing that the largest through-thickness variations in the deformation field take place near the free surface, the mesh is graded in the thickness direction such that the layer interfaces are at $x_3/h = 0.056, 0.139, 0.222, 0.333, 0.417, 0.472$ and 0.5 . The uniform line load through the thickness is imposed on top of the specimen while the vertical displacement at the two supports and the horizontal displacement on the line of the loading are constrained.

The main concern is investigating the extent of the deviation of the near tip stress or its gradient field from the corresponding plane-stress K -field and to compute the stress intensity factors along the three-dimensional crack fronts.

One of the most effective methods of generating the three components of the stress intensity factor from the fully mixed three-dimensional elastic deformation field, makes use of the interaction energy release rate formulation developed by Shih and Asaro (1989). Similar to the two-dimensional cases, the interaction energy in the three-dimensional configuration of cracks can be expressed as follows:

$$G_{\text{int}}(x_3) = \lim_{\Gamma \rightarrow 0} \int_{\Gamma(x_3)} \left[\sigma_{ij} \epsilon_{ij}^{\text{aux}} n_1 - \sigma_{ij} \frac{\partial u_i^{\text{aux}}}{\partial x_1} n_j - \sigma_{ij}^{\text{aux}} \frac{\partial u_i}{\partial x_1} n_j \right] d\Gamma, \quad (8)$$

where $\Gamma(x_3)$ denotes an open contour surrounding the crack front and lying on the plane $x_3 = \text{constant}$. Roman letters in subscripts range from 1 to 3. As in the two-dimensional formulation, the variables with the superscripts ‘‘aux’’ are the solutions of the auxiliary field. This interaction energy release rate is a conservation energy integral and it relates to stress intensity factors along the crack front line by

$$G_{\text{int}}(x_3) = \frac{2}{\dot{E} \cosh^2(\pi \epsilon_c)} [K_1 K_1^{\text{aux}} + K_2 K_2^{\text{aux}}] + \frac{1}{\dot{\mu}} K_3 K_3^{\text{aux}}, \quad (9)$$

where K_3^{aux} is the stress intensity factor for the auxiliary stress field of mode 3 at a point x_3 in addition to two-dimensional components K_1^{aux} and K_2^{aux} . It should be noted that unlike the plane stress case, discussed in eqn (9), a non-zero K_3 component may be present along

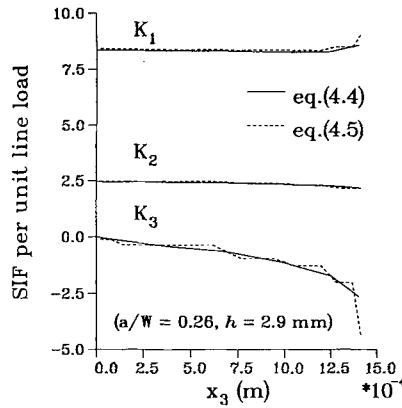


Fig. 6. Stress intensity factors obtained by two different computational techniques [see Section 4, eqns (11) and (12)].

portions of the crack front under complete three-dimensional conditions. The effective shear modulus of the bimaterial is

$$\frac{1}{\mu^*} = \frac{1}{2} \left(\frac{1}{\mu_1} + \frac{1}{\mu_2} \right). \quad (10)$$

The domain integral method due to Nakamura *et al.* (1989) is adopted for the more accurate evaluation of the interaction energy release rate, realizing that the computed fields near the tip may be rather inaccurate due to high deformation gradients. Here, we discuss two different formulations in computing the interaction energy. The first approach is based on the method by Shih *et al.* (1986), who computed the energy release rate of three-dimensional cracks. This was investigated and compared with other methods of computing stress intensity factors discussed by Li *et al.* (1985). The details of the first approach are provided in Nakamura *et al.* (1989). In this approach, G_{int} is expressed as:

$$G_{\text{int}}(x_3) = \frac{1}{h_{\text{el}}} \int_{V_0} \left[\sigma_{ij} \varepsilon_{ij}^{\text{aux}} \frac{\partial q}{\partial x_1} - \left(\sigma_{ij} \frac{\partial u_i^{\text{aux}}}{\partial x_1} + \sigma_{ij}^{\text{aux}} \frac{\partial u_i}{\partial x_1} \right) \frac{\partial q}{\partial x_j} \right] dV, \quad (11)$$

where V_0 is the volume enclosed by an arbitrarily chosen outer contour strip Γ_0 with thickness h_{el} . The continuous weighting function q vanishes at all points on the boundary of the volume V_0 except at the crack planes. For further details on this formulation, refer to Shih *et al.* (1986).

The second expression is obtained by changing the volume integration to an area integration by virtue of the divergence theorem G_{int} then becomes

$$G_{\text{int}}(x_3) = \int_{S_0} \left[\sigma_{ij} \varepsilon_{ij}^{\text{aux}} \frac{\partial q}{\partial x_1} - \left(\sigma_{i\beta} \frac{\partial u_i^{\text{aux}}}{\partial x_1} \sigma_{i\beta}^{\text{aux}} \frac{\partial u_i}{\partial x_1} \right) \frac{\partial q}{\partial x_\beta} + \left(\frac{\partial \sigma_{i3}}{\partial x_3} \frac{\partial u_i^{\text{aux}}}{\partial x_1} + \sigma_{i3}^{\text{aux}} \frac{\partial^2 u_i}{\partial x_1 \partial x_3} \right) q \right] dS, \quad (12)$$

where the gradients with respect to the out-of-plane coordinate appear only in the last parenthesis and can be computed by using smoothing techniques [see Hinton and Campbell (1974)]. The weighting function q is the same as the one used in the two-dimensional computation. In this calculation, a local smoothing technique was implemented to avoid the propagation of the discontinuities of stresses and strains along the interface planes. The two local stress intensity factors, at the quadrature points in the thickness direction, were thus computed. When eight-noded brick elements are used, as in the present study, the

number of locations where the local stress intensity factors are computed in the first expression, are approximately half of those of the second expression. This is because the number of quadrature points in the thickness direction is approximately twice as many as the number of nodal points. In Fig. 6, the comparison of two formulations for the interaction energy is presented. Excellent agreement between the two formulations is shown.

Optical methods such as Twyman–Green interferometry, caustics and Cherenkov Gradient Sensing (CGS) rely on the net optical path difference accumulated by thickness changes caused by the crack-tip singularity and stress-induced changes of the refractive index of the material. For an isotropic transparent material, the following expression provides the relation between the optical path difference δS acquired during refraction of a collimated light bundle through the uniform specimen thickness [see Rosakis *et al.* (1990) and Rosakis (1992)]:

$$\delta S = c_\sigma h \int_{-1/2}^{1/2} \left\{ (\sigma_{11} + \sigma_{22}) \left[1 + \frac{\sigma_{33}}{\nu(\sigma_{11} + \sigma_{22})} \right] \right\} d(x_3/h), \quad (13)$$

where c_σ is the stress-optic constant of the material and h is the thickness of the plate. As is evident from eqn (13), for either a homogeneous or a bimaterial cracked linear elastic plate of uniform thickness and finite in-plane dimensions, the optical path difference δS (transparent specimen) in general will depend on the details of the three-dimensional elastostatic or elastodynamic stress state that would exist in the vicinity of the crack tip. This will be a function of the specimen geometry and loading. For bimaterial systems, it is also expected to depend on the material mismatch.

Given the lack of full-field three-dimensional analytical solutions in fracture mechanics, experimental information can strictly be extracted by means of detailed numerical calculations. Nevertheless, there exist certain non-trivial special cases for which available asymptotic solutions, based on two-dimensional analyses, may provide adequate approximation for δS at a certain region near the crack tip. In particular it has been argued that conditions of plane stress will dominate in thin *homogeneous* cracked plates at distances from the crack front larger than half the specimen thickness. This would imply that if only fringes outside the three-dimensional zone are analysed the results could be interpreted on the basis of a plane stress analysis [see Rosakis and Ravi-Chandar (1986) and Rosakis (1992)]. An equivalent issue arises in the case of a crack in an interface between two different materials. Equation (13) is written in such a way that the second term in the square brackets, $\sigma_{33}/\nu(\sigma_{11} + \sigma_{22})$, is identified as the degree of plane strain. The degree of plane strain is a measure of three-dimensionality near the crack tip. This measure is equal to zero under strict plane stress conditions and is equal to one under perfect plane strain conditions. At points in the specimen where plane stress is a good approximation, that term can be neglected and eqn (13) reduces to,

$$\delta S \sim c_\sigma h (\bar{\sigma}_{11} + \bar{\sigma}_{22}), \quad (14)$$

where $(\bar{\sigma}_{11} + \bar{\sigma}_{22})$ is the thickness average of the hydrostatic stress under plane stress conditions. The fringe order is proportional to δS for a Twyman–Green interferometer, and is proportional to the derivative of δS in the shearing direction for CGS. Caustics are also related to both gradient components of $(\bar{\sigma}_{11} + \bar{\sigma}_{22})$.

To illustrate the extent of the near-tip three-dimensionality, reference is made to Fig. 7 which shows a three-dimensionality representation of the ratio $\sigma_{33}/\nu(\sigma_{11} + \sigma_{22})$ for a three-point bend specimen of a homogeneous material. The ratio is a measure of near-tip three-dimensionality and is obtained by means of a three-dimensional finite element calculation which models a stationary crack in a three-point bend specimen. In the figure, only one half of the specimen thickness is shown. The top surface corresponds to the mid-plane of the specimen. The traction-free crack face is on the left-hand side of the picture. The maximum extent of the three-dimensional zone is approximately $0.4 \sim 0.5h$ at $\theta = 0^\circ$, while at $\theta \approx 120^\circ$, the plane stress approximation is adequate very close to the crack tip, say $r \approx 0.1h$ [for details, see Krishnaswamy *et al.* (1991)].

For a bimaterial system an equivalent calculation can be made. Figures 8(a) and (b) provide two views of the ratio $\sigma_{33}/\nu_1(\sigma_{11} + \sigma_{22})$ (ν_1 is Poisson's ratio for PMMA) for the PMMA/aluminum systems described above. In Fig. 8(a), the ratio is plotted for the specimen mid-plane. The top side corresponds to PMMA and the crack surface is visible in the left-hand side of the picture. Figure 8(b) gives a three-dimensional view of the PMMA side which is relevant for the analysis of the transmission CGS patterns. Here again the top surface of the three-dimensional mesh corresponds to the specimen mid-plane. As is obvious from a comparison of Figs 7 and 8(b), the nature of the three-dimensional deformation in bimetals is different to that of homogeneous systems. As is obvious from Figs 8(a) and (b), the three-dimensional zone extends along the PMMA/aluminum bond line. Unlike the homogeneous case there exists no plane stress region at any visible distance directly ahead of the crack tip. Here, plane stress conditions are achieved above a strip of height, roughly equal to $0.4h$, lying ahead of the tip in the PMMA side. In addition, there exists a narrow wedge of plane stress defined by $100^\circ < \theta < 150^\circ$, $r < 0.1h$. Close scrutiny of Fig. 8(a) reveals that the extent of the near-tip three-dimensional zone in the aluminum side is slightly smaller than the PMMA side. Unfortunately, this fact cannot be exploited here since the aluminum side also experiences very little deformation thus making the application of optical methods difficult.

Figures 9(a) and (b) show a comparison between the three-dimensional zones corresponding to a/W ratios of 0.2 and 0.4 for the same specimen thickness, h , specimen width, W , and specimen length, L . As is evident from these figures, the shape and extent of the three-dimensional zone remains insensitive to a/W for this range of a/W . The effect of specimen thickness on the near-tip three-dimensional zone is illustrated if Fig. 9(b) is compared to Fig. 9(c). Figure 9(c) shows the ratio $\sigma_{33}/\nu_1(\sigma_{11} + \sigma_{22})$ for a specimen of the same in-plane dimensions as in Fig. 9(b) but of half the plate thickness. As expected the extent of the three-dimensional zone scales with specimen thickness. This is an important observation regarding optical experiments. Indeed the outer boundary of dominance of the plane stress K -field is only sensitive to the in-plane specimen dimensions and as a result a reduction of test specimen thickness may allow for the establishment of such a field around a reduced near-tip three-dimensional zone.

Figure 10 illustrates the establishment of a plane stress K -field outside the near-tip three-dimensional zone, for a specific thickness ($h = 2.9$ mm) and $a/W = 0.26$. The top figure shows the experimentally obtained CGS fringe pattern. The bottom figure compares the digitized experimental result (open circles) to the synthetic contours of $\partial(\bar{\sigma}_{11} + \bar{\sigma}_{22})/\partial x_1$ corresponding to a plane stress K -field. The values of K_1 and K_2 are chosen by matching the experimental points, outside the three-dimensional zone, to the K -field asymptotic solution. The two sets of fringes agree well at points away from the bond line and crack flanks as expected from the shape of the three-dimensional zone in Figs 8 and 9. For the loops centered at $\theta \approx 135^\circ$, disagreement at points furthest from the crack tip indicates that higher order terms in the asymptotic expansion might be influencing the experimental fringe pattern. Nevertheless, there exists a substantial region surrounding the tip where the agreement is excellent. This is further corroborated by the fact that K_1 and K_2 values obtained by the fit were very close to the numerically obtained, plane stress equivalents. To further illustrate this effect, Fig. 11 compares contours of hydrostatic stress obtained by means of the three-dimensional numerical calculation and the asymptotic plane stress field for the same specimen geometry as in Fig. 10. The results show the establishment of a well-defined K -field outside the three-dimensional zone.

5. RELATION BETWEEN THE FAR AND NEAR TIP FIELDS

In Section 4, the extent of the near-tip three-dimensional zone was investigated for the case of a crack in a bimaterial interface. It was further shown that under certain circumstances (mainly related to specimen thickness) a plane stress K -field may be established outside the near-tip three-dimensional zone. In an experimental situation we rely on the establishment of such a plane stress K -field for the evaluation of the plane stress values of the components of the complex stress intensity factor K^σ . Since the goal of experiments is

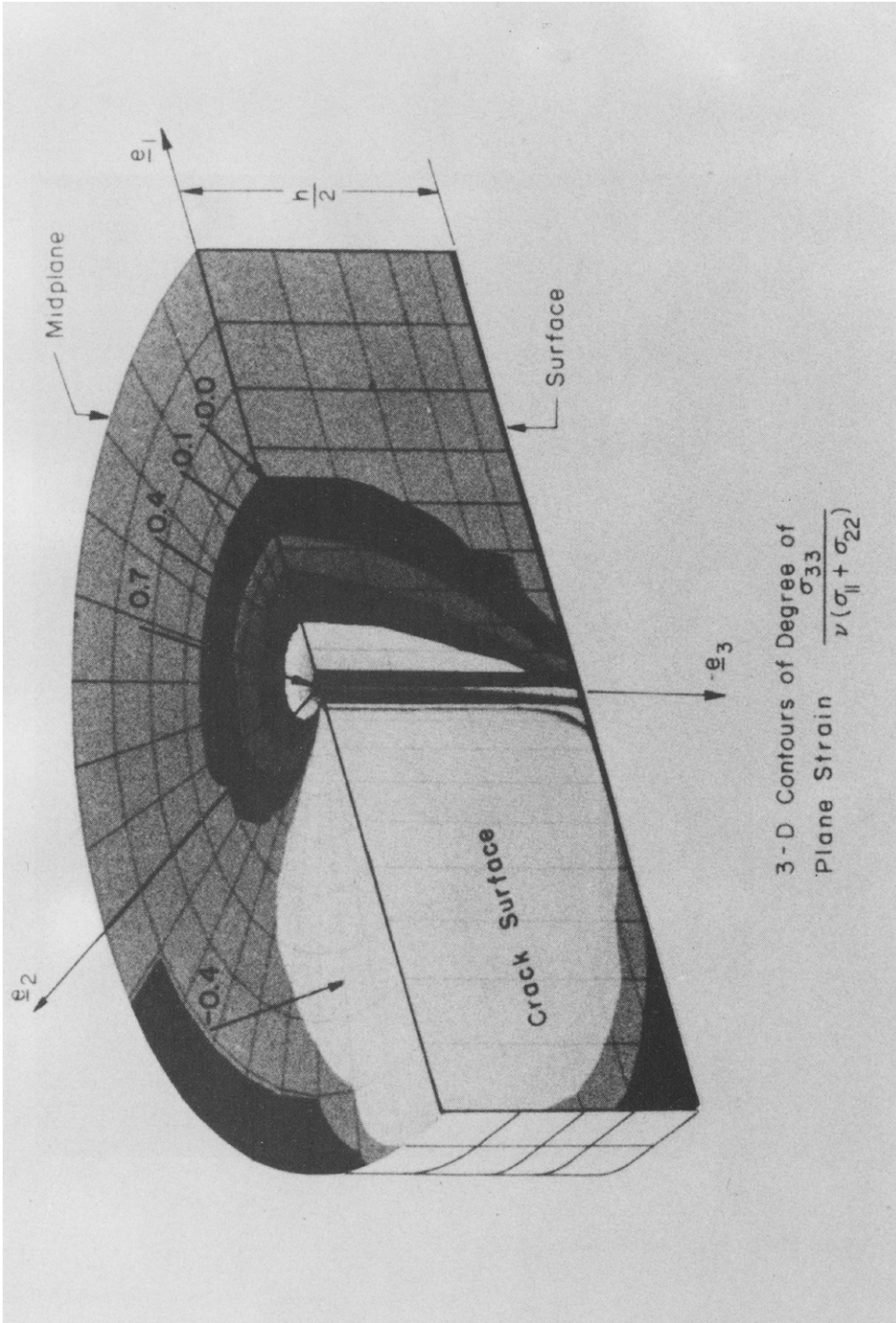


Fig. 7. Color contour plot of the degree of plane strain ($\sigma_{33}/\nu(\sigma_{11} + \sigma_{22})$) at the vicinity of a symmetrically loaded crack in a homogeneous elastic plate : three-dimensional view.

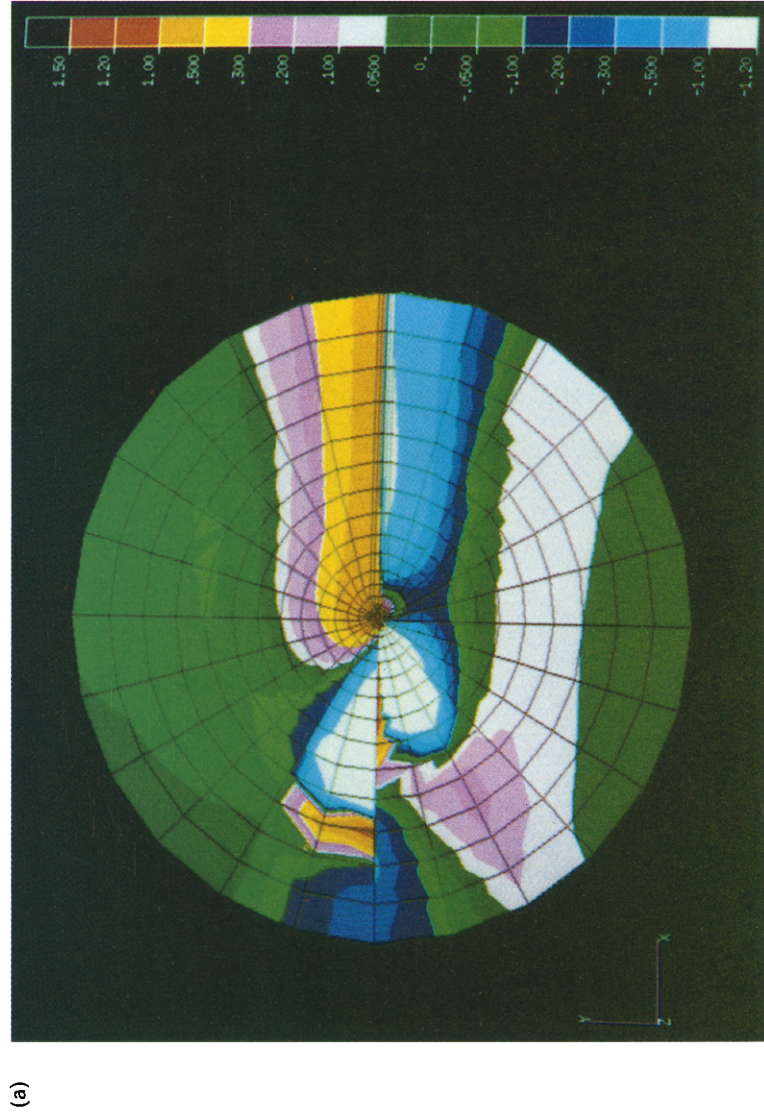
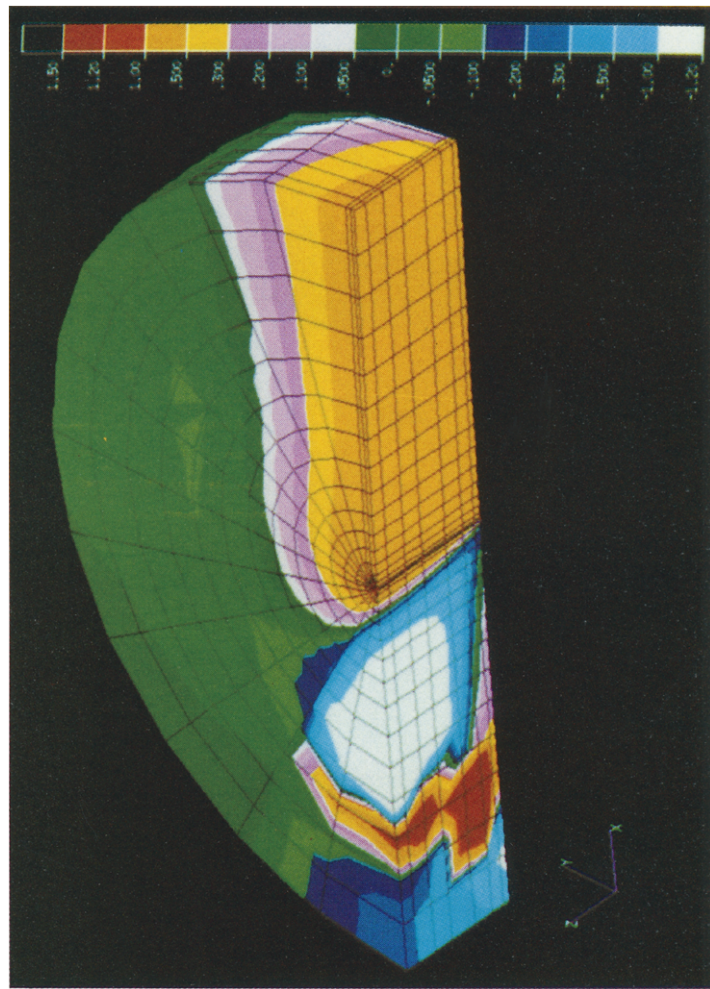


Fig. 8. Color contour plots of the degree of plane strain ($\sigma_{33}/\nu(\sigma_{11} + \sigma_{22})$) in the vicinity of an interfacial crack in a bimaterial plate: (a) two-dimensional view on the mid-plane (top : PMMA ; bottom : aluminum), and (b) three-dimensional view in PMMA side.



(b)

(Fig. 8. Continued)

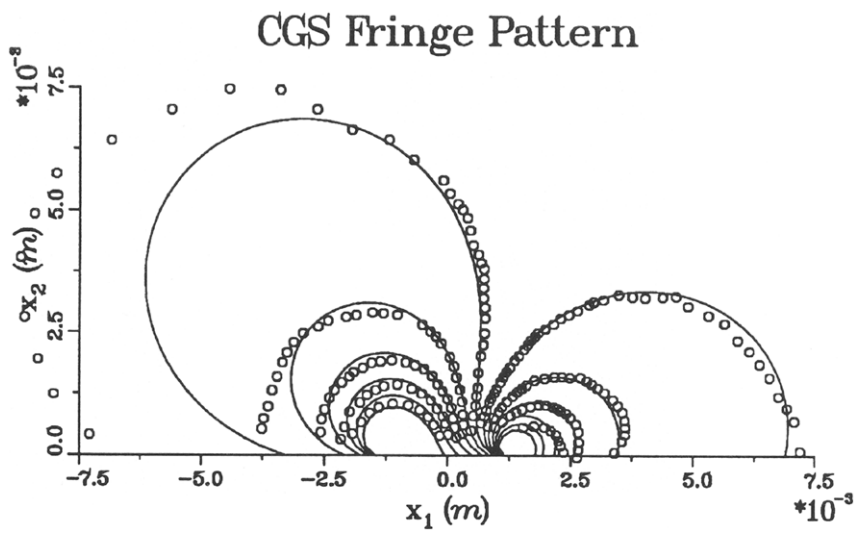
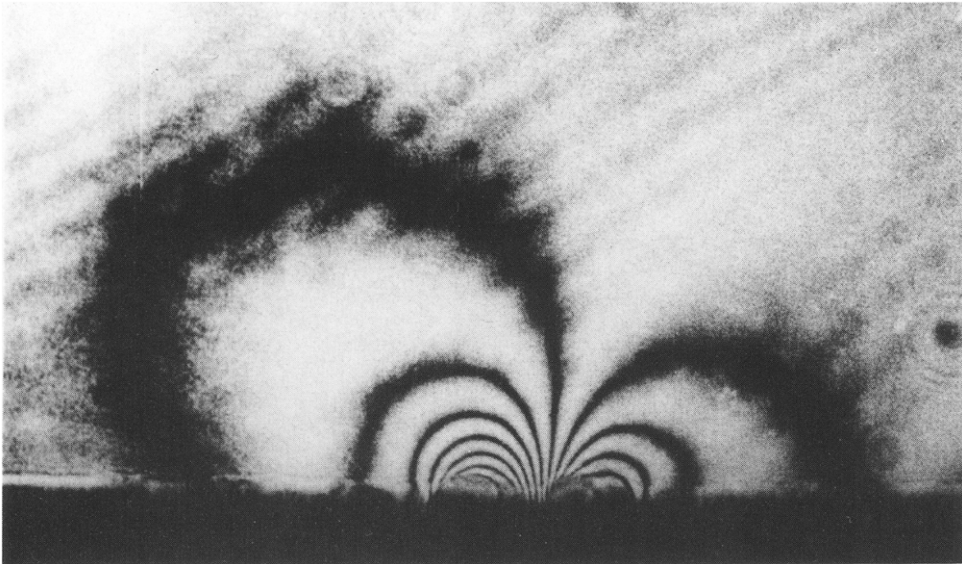


Fig. 10. Comparison between experimentally obtained and synthetically constructed, x_1 -gradient CGS interferograms ($a/W = 0.26$, $h = 2.9$ mm). Open circles designate digitized fringe locations of photograph. Solid lines represent CGS fringes predicted by means of a complex plane stress K -field.

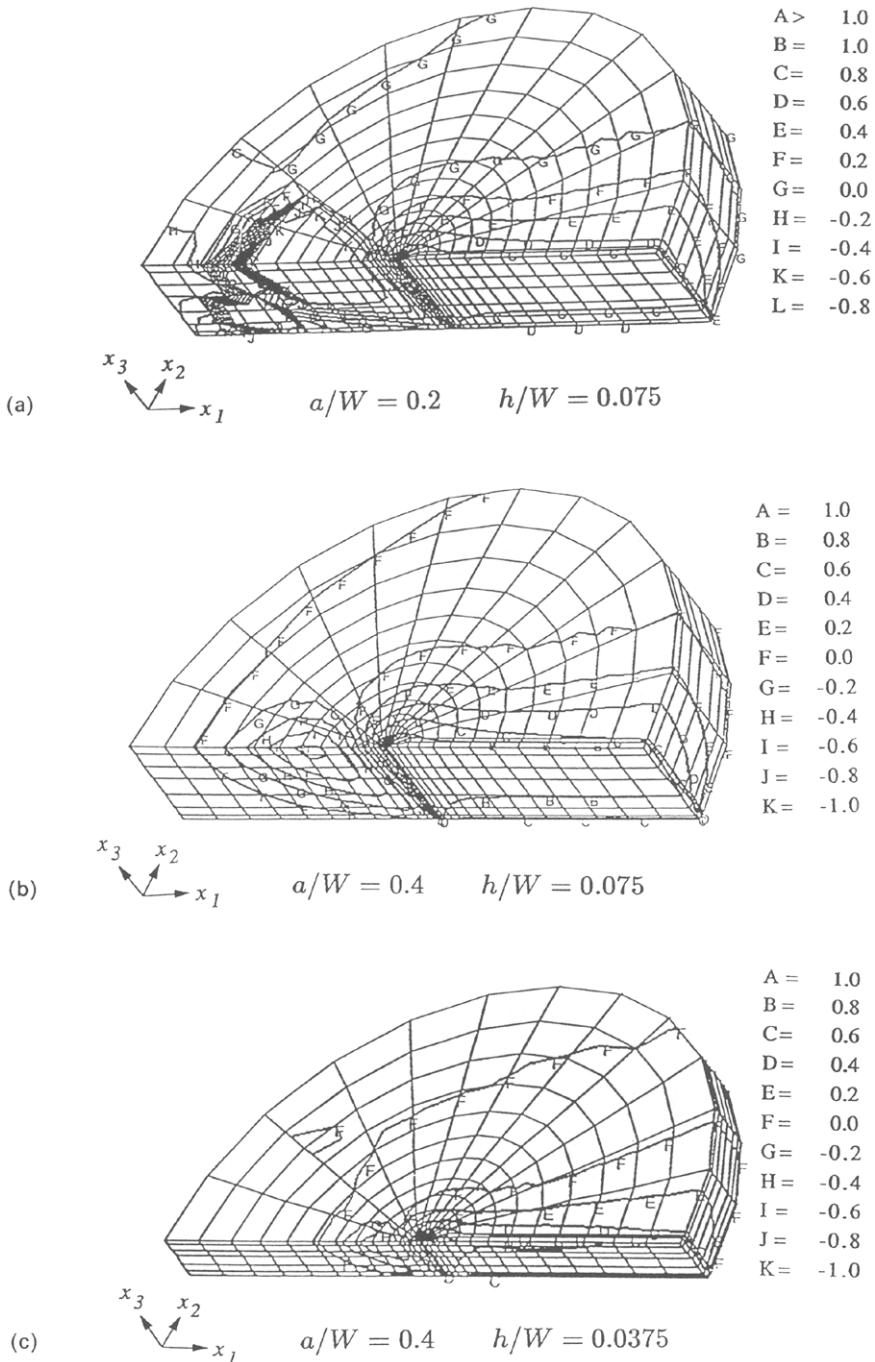


Fig. 9. Three-dimensional contour map showing the degree of plane strain in the near tip region of a three point bend, PMMA/aluminum, bimaterial specimen: (a) $a/W = 0.2$, (b) $a/W = 0.4$ for a plate thickness of 9 mm, and (c) $a/W = 0.2$ for a plate thickness of 4.5 mm.

to be able to formulate crack initiation and growth criteria, K^σ has to be related to a more local quantity that determines the behavior near the crack front where plane strain conditions dominate. Such a quantity may be K^ϵ which is the plane strain equivalent of K^σ . In addition, a means of scaling the results obtained from experimentation in thin specimens of a specific thickness to K^σ -dominant specimens of any thickness should be available. To achieve the above-mentioned goals, a three-dimensional boundary-layer type of calculation is performed here. A semi-infinite interfacial crack in an infinite bimaterial plate of unit thickness is modeled. The bimaterial is composed of PMMA and aluminum. At a radial

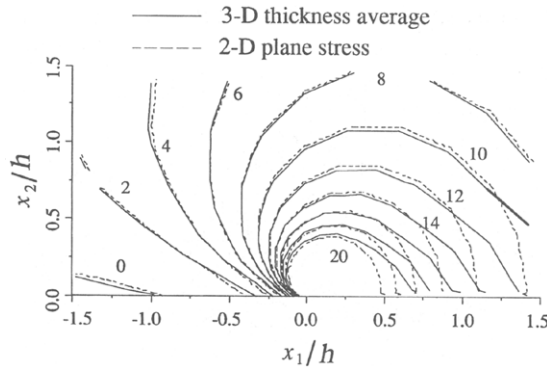


Fig. 11. Comparison of hydrostatic stress contours near a crack tip in PMMA/aluminum specimens : three-dimensional full-field (dashed lines), two-dimensional plane stress full-field (dotted lines) and two-dimensional plane stress K -field (solid lines). Note that the dashed and dotted lines are completely overlapped in almost all regions.

distance of 10 thicknesses away from the crack front, the plane stress K -field is applied as a remote boundary condition. The three-dimensional mesh is shown in Fig. 12. The total number of elements used in this computation was 3344 and 10 layers of elements are used in the thickness direction.

Our purpose here is to relate the amplitude of the far-field (plane stress) complex stress intensity factor K^σ to the near-tip (plane strain) thickness average equivalent K_{ave}^e . These are expressed here as

$$K^\sigma = |K^\sigma| e^{i\psi^\sigma}, \quad \text{and} \quad K_{ave}^e = |K_{ave}^e| e^{i\psi_{ave}^e}. \tag{15}$$

In the above expressions, the subscript “ave” means a plate thickness average as follows :

$$K_{ave}^e = \int_{-1/2}^{1/2} K^e(x_3) d(x_3/h), \quad \text{and} \quad K^e(x_3) = |K^e(x_3)| e^{i\psi^e(x_3)}, \tag{16}$$

where $K^e(x_3)$ is the local value of the plane strain, complex stress intensity factor along the crack front and $\psi^e(x_3)$ is the local value of the phase angle. It should be emphasized that

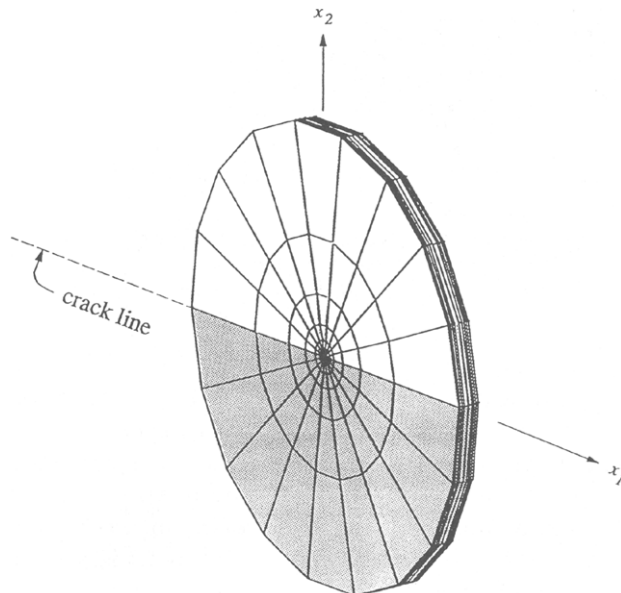


Fig. 12. Mesh geometry used in the three-dimensional boundary-layer type of computations.

unlike homogeneous fracture specimens, in the bimaterial case, the far-field phase angle ψ^σ and the near-tip thickness average phase angle ψ_{ave}^ε are not the same. This is true since in the bimaterial case, the asymptotic field cannot be decomposed in two distinct uncoupled modes of specific symmetries.

Application of the three-dimensional version of the path-independent surface integral J_{ave} evaluated over two cylindrical surfaces through the plate thickness, surrounding the entire crack front, provides the following relation :

$$\frac{|K^\sigma|^2}{\overset{*}{E}} = \int_{-1/2}^{1/2} \left[\frac{|K^\varepsilon(x_3/h)|^2}{\overset{*}{E}'} + \frac{|K_3(x_3/h)|^2}{2\overset{*}{\mu}} \right] d(x_3/h), \tag{17}$$

where $\overset{*}{E}'$ is the effective Young's modulus adjusted to the plane stress conditions by substituting for ν_α with the quantities $\nu_\alpha/(\nu_\alpha + 1)$ in the last term of eqn (5). The contribution of the second term in the right-hand side of eqn (17) is expected to be smaller than the first term provided that in-plane loading conditions are prescribed. Thus the above equation can be approximated as :

$$\frac{|K^\sigma|^2}{\overset{*}{E}} = \frac{|K_{ave}^\varepsilon|^2}{\overset{*}{E}'}. \tag{18}$$

However, not only the magnitude of the complex stress intensity factor but also the phase angles differ between the plane stress far-field and the average plane strain near-tip field due to the oscillatory nature of the stresses in bimetals. Indeed even the oscillatory indexes for these two fields are different. Near the crack-tip, conditions of plane strain prevail and thus the oscillatory index is given by ε_σ . At the far-field, conditions of plane stress are dominant and this index is given by ε_σ .

The relation between the complex values of K^σ and K_{ave}^ε are furnished by means of the three-dimensional numerical calculation described above. In this calculation the only length scale present is the plate thickness. We can thus normalize the spatial coordinates of the near-tip field with the thickness. The tractions on the annular plane stress outer boundary are expressed as follows :

$$\begin{aligned} \sigma_{22} + i\sigma_{12} &= \frac{|K^\sigma| e^{i(\psi^\sigma + \varepsilon_\sigma \ln r)}}{\sqrt{2\pi r}} \\ &= \frac{\mu^{(1)} |\hat{K}^\sigma| e^{i(\hat{\psi}^\sigma + \varepsilon_\sigma \ln r/h)}}{\sqrt{2\pi r/h}}, \end{aligned} \tag{19}$$

where variables with a superposed hat represent the normalized quantities. In the numerical calculation, the external strip of the boundary is subjected to the traction of a normalized plane stress bimaterial K -field of unit magnitude, i.e. $|\hat{K}^\sigma| = 1$, and given phase angle $\hat{\psi}^\sigma$. The thickness average near-tip plane strain K -field can also be normalized by h and $\mu^{(1)}$ in a similar fashion. In addition, the oscillatory index is now given by ε_σ rather than ε_σ in the oscillatory index. The relations between the original and normalized complex stress intensity factor magnitudes and phase angles for both the far field and average near-tip field are given by

$$\begin{aligned} |K^\sigma| &= |\hat{K}^\sigma| \mu^{(1)} \sqrt{h}, \\ |K_{ave}^\varepsilon| &= |\hat{K}_{ave}^\varepsilon| \mu^{(1)} \sqrt{h}, \end{aligned} \tag{20}$$

and

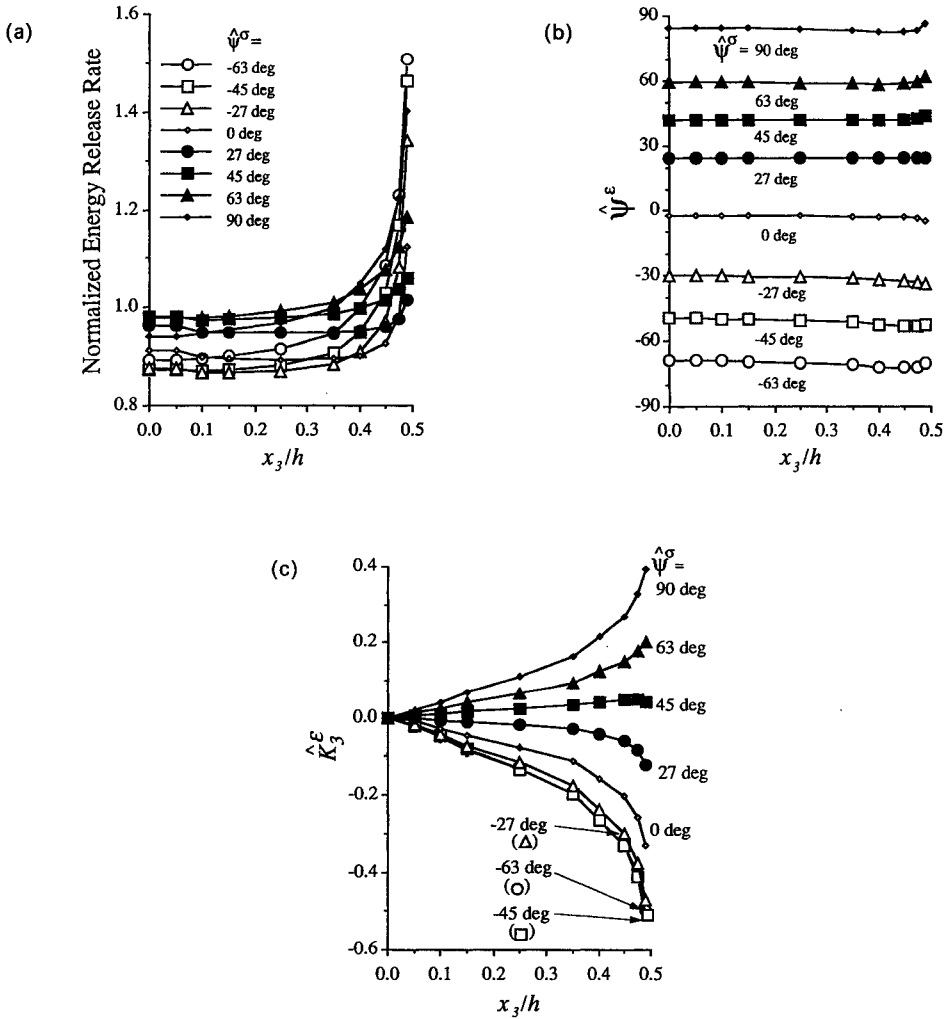


Fig. 13. Normalized local near-tip, plane strain, field quantities for a normalized remote plane stress K -field of various phase angles: (a) normalized local energy release rate, (b) plane strain phase angle $\hat{\psi}^\sigma(x_3)$, and (c) mode 3 stress intensity factor \hat{K}_3^ϵ .

$$\begin{aligned} \psi^\sigma &= \hat{\psi}^\sigma - \epsilon_\sigma \ln h, \\ \psi^\epsilon_{ave} &= \hat{\psi}^\epsilon_{ave} - \epsilon_\epsilon \ln h. \end{aligned} \tag{21}$$

The average near-tip phase angles, $\hat{\psi}^\epsilon_{ave}$, are computed for the given far-field phase angle $\hat{\psi}^\sigma$ by using the method described in Section 4 which provides the local value of \hat{K}^ϵ and $|\hat{\psi}^\epsilon$. The average values are given by integrating $|\hat{K}^\epsilon(x_3)|$ and $\hat{\psi}^\epsilon(x_3)$ along the x_3 -axis.

Figures 13(a), (b) and (c) give the local distribution of the normalized energy release rate, phase angle $\hat{\psi}^\sigma(x_3/h)$, and $K_3(x_3/h)$ respectively across the specimen thickness. In each figure, results corresponding to a variety of remotely applied phase angles $\hat{\psi}^\sigma$ of the normalized plane stress K -field are shown. The complete range of far-field mixities from $\hat{\psi}^\sigma = 90^\circ$ to $\hat{\psi}^\sigma = -90^\circ$ is covered. In Fig. 13(a), the normalized energy release rate remains uniform through most of the plate thickness but experiences a drastic increase as the specimen surface is approached. This fact may be related to the experimental observation by Liechti and Chai (1990) who reported curved crack fronts in bimetals which are concave in the direction of the crack growth. Figure 13(b) shows the variation of local normalized $\hat{\psi}^\sigma$ across the crack front. The flatness of these curves is remarkable, suggesting that $\hat{\psi}^\sigma \approx \hat{\psi}^\sigma_{ave}$. Finally, Fig. 13(c) gives the thickness variation of the normalized \hat{K}_3^ϵ along the crack front. It is interesting to note that although the far-field plane stress loading is purely in-plane, three-dimensional effects are also demonstrated near the crack front in terms of out-of-plane deformation near the specimen free surface.

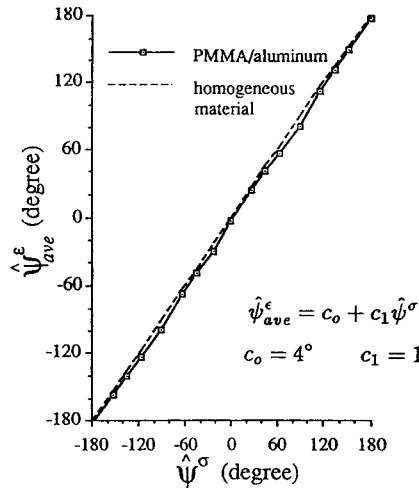


Fig. 14. The variation of $\hat{\psi}_{ave}^\epsilon$, the near-tip plane strain phase angle averaged through the plate thickness, with the remotely applied plane stress equivalent, $\hat{\psi}^\sigma$.

In Fig. 14, the relation between $\hat{\psi}^\sigma$ and $\hat{\psi}_{ave}^\epsilon$ both for a homogeneous material and a PMMA/aluminum bimaterial is shown. The relation between $\hat{\psi}^\sigma$ and $\hat{\psi}_{ave}^\epsilon$ in the homogeneous material is linear, as expected, while the bimaterial case is also very close to being linear. For the bimaterial case, the relation can be approximated as follows :

$$\hat{\psi}_{ave}^\epsilon = c_0 + c_1 \hat{\psi}^\sigma, \tag{22}$$

where $c_0 \approx 5^\circ$ and $c_1 \approx 1$ in the PMMA/aluminum bimaterial. Although the coefficients c_0 and c_1 are expected to depend on the specifics of the bimaterial combination used, we anticipate that for most bimaterials, $c_0 \approx 0^\circ$ and $c_1 \approx 1$, since the bimaterial considered here corresponds to extremes in stiffness mismatch between the two sides.

Given the above, eqns (21) and (22) furnish a relation between the non-normalized far-field and near-tip phase angles as follows :

$$\psi^\epsilon \approx \psi^\sigma + (\epsilon_\sigma - \epsilon_c) \ln h, \tag{23}$$

where $c_0 \approx 0^\circ$ and $c_1 \approx 1$. The validity of the above relation in a special case can be checked by taking a close look at the results obtained by Nakamura (1991) who considered the case of a bimaterial system with $\epsilon_c = 0$. He computed the increment of the near-tip phase angle by decreasing the thickness of a center-cracked panel where $\epsilon_\sigma = -0.033$ and $\mu_1/\mu_2 = 3$. The phase angle increment was about 4.3° for every decade decrease in thickness [see Fig. 7(a) in Nakamura (1991)]. Our proposed relation in eqn (23) predicts the same change in ψ_{ave}^ϵ for this special case. Our numerical results for the three-point bend specimen geometry also support the validity of the above relation in a totally different bimaterial combination and specimen geometry.

The above simple expressions, eqns (18) and (23), allow us to relate the experimentally measurable plane stress K^σ to the average near-tip K_{ave}^ϵ which may be a more relevant parameter in the formulation of a fracture criterion. In addition, relation (23) also provides a means of comparing the results obtained between specimens with different thicknesses.

6. CONCLUSIONS

In the first part of this work, a PMMA-aluminum bimaterial specimen of the three-point bend type was modeled by means of three-dimensional and plane stress calculations. The analyses provided information regarding the regions near the crack tip where data collected by optical measurements can be used to extract fracture parameters in specimens

of various crack lengths and thicknesses. The results indicated that severe near-tip three-dimensionality surrounds most of the near-tip region (up to half of the specimen thickness) and extends along the interface (strip of width equal to half of the specimen thickness). The existence of a plane stress K -dominant region was investigated.

The second set of calculations concentrated on establishing a relation between the far-field plane stress and the near-tip plane strain complex stress intensity factors in bimaterial plates. This relation allows for the scaling of results obtained by experimentation in K -dominant plates of various thicknesses.

Acknowledgements—The support of the National Science Foundation Contract MSS-9024838 and the Office of Naval Research N00014-90-J-1340 is gratefully acknowledged. The computations were performed using the facilities of the San Diego Supercomputer Center and at the Jet Propulsion Laboratory Supercomputing Project.

REFERENCES

- Barsoum, R. S. and Chen, T.-K. (1991). Three-dimensional surface singularity of an interface crack. *Int. J. Fract.* **50**, 221–237.
- Beinert, J. and Kalthoff, J. F. (1981). Experimental determination of dynamic stress intensity factors by the method of shadow patterns. In *Mechanics of Fracture* (Edited by G. C. Sih), Vol. 7, pp. 281–330. Martinus Nijhoff, London.
- Bogy, D. B. (1971). Two edge-bonded elastic wedges of different materials and wedge angles under surface tractions. *J. Appl. Mech.* **38**, 377–386.
- Gharhmani, F. and Shih, C. F. (1992). Corner singularities of three-dimensional planar interfacial cracks. *J. Appl. Mech.* **59**, 61–68.
- Hinton, E. and Campbell, J. S. (1974). Local and global smoothing of discontinuous finite element functions using a least square method. *Int. J. Numer. Meth. Engng* **8**, 461–480.
- Kim, K. S. (1985). A stress intensity factor tracer. *J. Appl. Mech.* **52**, 291–297.
- Krishnaswami, S., Rosakis, A. J. and Ravichandran, G. (1991). On the extent of dominance of asymptotic elastodynamic crack-tip fields: Part II. Numerical investigation of three-dimensional and transient effects. *J. Appl. Mech.* **58**, 95–103.
- Lee, Y. J. and Rosakis, A. J. (1993). Interfacial cracks in plates: An experimental investigation (in preparation).
- Li, F. Z., Shih, C. F. and Needleman, A. (1985). A comparison of methods for calculating energy release rates. *Engng Fract. Mech.* **21**, 405–421.
- Liechti, K. M. and Chai, Y.-S. (1990). Three dimensional effects in interfacial crack growth. *Appl. Mech. Rev.* **43**, S271–S273.
- Nakamura, T. (1991). Three-dimensional stress fields of elastic interface cracks. *J. Appl. Mech.* **58**, 1411–1426.
- Nakamura, T. and Parks, D. M. (1988). Three-dimensional stress field near the crack front of a thin elastic plate. *J. Appl. Mech.* **55**, 805–813.
- Nakamura, T. and Parks, D. M. (1989). Antisymmetrical 3-D stress field near the crack front of a thin elastic plate. *Int. J. Solids Structures* **25**, 1411–1426.
- Nakamura, T., Shih, C. F. and Freund, L. B. (1989). Three-dimensional transient analysis of a dynamically loaded three-point-bend ductile fracture specimen. *ASTM Nonlinear Fracture Mechanics* **1**, STP **995**, 217–241.
- Narasimhan, R. and Rosakis, A. J. (1988). Three dimensional effects near a crack tip in a ductile three point bend specimen. Part I. Numerical analysis. *J. Appl. Mech.* **57**, 607–617.
- Parsons, I. D., Hall, J. F. and Rosakis, A. J. (1986). A finite element investigation of the elastostatic state near a three-dimensional edge crack. GALCIT Report SM 86-29, California Institute of Technology.
- Post, D. (1987). Moiré interferometry. In *Handbook on Experimental Mechanics* (Edited by A. S. Kobayashi), Chap. 7. Prentice-Hall.
- Rosakis, A. J. (1993). Two optical techniques sensitive to gradients of optical path difference: The method of caustics and the coherent gradient sensor (C.G.S). In *Experimental Techniques in Fracture* (Edited by J. Epstein), Vol. 3. VCH Publishers, New York.
- Rosakis, A. J., Krishnaswami, S. and Tippur, H. V. (1990). On the application of the optical method of caustics to the investigation of transient elastodynamic crack problems: Limitations of the classical interpretation. *J. Opt. Lasers Engng* **13**, 183–210.
- Rosakis, A. J., Lee, Y. J. and Lambros, J. (1991). Dynamic crack growth in bimaterial interfaces. *ASME AMD* **130**, 17–23.
- Rosakis, A. J. and Ravi-Chandar, K. (1986). On crack-tip stress states: An experimental evaluation of three-dimensional effects. *Int. J. Solids Structures* **22**, 121–134.
- Shih, C. F. and Asaro, R. J. (1989). Elastic-plastic analysis of cracks on bimaterial interfaces: Part I. Small scale yielding. *J. Appl. Mech.* **55**, 299–316.
- Shih, C. F., Moran, B. and Nakamura, T. (1986). Energy release rate along a three-dimensional crack front in a thermally stressed body. *Int. J. Fract.* **30**, 79–102.
- Stern, M., Becker, E. B. and Dunham, R. S. (1976). A contour integral computation of mixed mode stress intensity factors. *Int. J. Fract.* **12**, 359–368.
- Tippur, H. V., Krishnaswami, S. and Rosakis, A. J. (1991). Optimal mapping of crack tip deformations using the methods of transmission and reflection coherent gradient sensing. *Int. J. Fract.* **52**, 91–117.
- Tippur, H. V. and Rosakis, A. J. (1991). Quasi-static and dynamic crack growth along bi-material interfaces: A note on crack tip field measurements using coherent gradient sensing. *Exper. Mech.* **31**, 243–251.
- Yau, J. F., Wang, S. S. and Corten, H. T. (1980). A mixed-mode crack analysis of isotropic solids using conservation laws of elasticity. *J. Appl. Mech.* **47**, 335–341.